

LONG TERM STABILITY AND DYNAMICAL ENVIRONMENT OF THE PSR 1257+12 PLANETARY SYSTEM

KRZYSZTOF GOŁDZIEWSKI¹

Toruń Centre for Astronomy, N. Copernicus University, Gagarina 11, 87-100 Toruń, Poland

MACIEJ KONACKI²

Department of Geological and Planetary Sciences, California Institute of Technology, MS 150-21, Pasadena, CA 91125, USA
 Nicolaus Copernicus Astronomical Center, Polish Academy of Sciences, Rabiańska 8, 87-100 Toruń, Poland

ALEX WOLSZCZAN³

Department of Astronomy and Astrophysics, Penn State University, University Park, PA 16802, USA
 Toruń Centre for Astronomy, Nicolaus Copernicus University ul. Gagarina 11, 87-100 Toruń, Poland
Draft version February 2, 2008

ABSTRACT

We study the long-term dynamics of the PSR 1257+12 planetary system. Using the recently determined accurate initial condition by Konacki & Wolszczan (2003) who derived the orbital inclinations and the absolute masses of the planets B and C, we investigate the system stability by long-term, 1 Gyr direct integrations. No secular changes of the semi-major axes, eccentricities and inclinations appear during such an interval. This stable behavior is confirmed with the fast indicator MEGNO. The analysis of the orbital stability in the neighborhood of the nominal initial condition reveals that the PSR 1257+12 system is localized in a wide stable region of the phase space but close to a few weak 2 and 3-body mean motion resonances. The long term stability is additionally confirmed by a negligible exchange of the Angular Momentum Deficit between the innermost planet A and the pair of the outer planets B and C. An important feature of the system that helps sustain the stability is the secular apsidal resonance (SAR) between the planets B and C with the center of libration about 180°. We also find useful limits on the elements of the innermost planet A which are otherwise unconstrained by the observations. Specifically, we find that the line of nodes of the planet A cannot be separated by more than about ±60° from the nodes of the bigger companions B and C. This limits the relative inclination of the orbit of the planet A to the mean orbital plane of the planets B and C to moderate values. We also perform a preliminary study of the short-term dynamics of massless particles in the system. We find that a relatively extended stable zone exists between the planets A and B. Beyond the planet C, the stable zone appears already at distances 0.5 AU from the parent star. For moderately low eccentricities, beyond 1 AU, the motion of massless particles does not suffer from strong instabilities and this zone is basically stable, independent on the inclinations of the orbits of the test particles to the mean orbital plane of the system. It is an encouraging result supporting the search for a putative dust disk or a Kuiper belt, especially with the SIRTF mission.

Subject headings: celestial mechanics, stellar dynamics—methods: numerical, N-body simulations—planetary systems—stars: individual (PSR 1257+12)

1. INTRODUCTION

Up to date, among about 130 extrasolar planetary systems, the one around PSR 1257+12 remains the only one which contains Earth-sized planets (Wolszczan & Frail 1992; Wolszczan 1994; Konacki & Wolszczan 2003). It has been discovered with the pulsar timing technique that relies on extremely precise measurements of the times of arrival (TOA) of pulsar pulses. Such a technique in principle allows a detection of companions as small as asteroids. In the case of the PSR B1257+12 it enabled the detection of three planets A, B and C with the orbital periods of 25, 66 and 98 days and the masses in the Earth-size regime (see Table 1). Luckily, the two larger planets have the mean motions close to the 3:2 commensurability which result in observable deviations from a simple Keplerian description of the motion (Rasio et al. 1992; Malhotra et al. 1992; Peale 1993; Wolszczan 1994; Konacki et al. 1999). Konacki & Wolszczan (2003) applied

the secular orbital theory of the PSR 1257+12 system from Konacki et al. (2000) to determine the masses and absolute inclinations of the orbits of the planets B and C. Recently, the same idea of incorporating the effects of mutual interactions between planets to remove the Doppler radial velocity (RV) signal degeneracy present in the *N*-Keplerian orbital model (i.e., the undeterminacy of the system inclination and the relative inclination of the orbits) has also been applied to study the strongly interacting, resonant system around Gliese 876 (Laughlin & Chambers 2001; Rivera & Lissauer 2001). However, the accuracy of the timing observations by far exceeds the precision of the RV measurements. In consequence, the accuracy of the PSR 1257+12 fit obtained by Konacki & Wolszczan (2003) and hence the initial condition is superior to any initial condition derived from the fits to RV observations of solar-type stars with planets. Thus, the system constitutes a particularly convenient and interesting subject for the studies of its dynamics.

There have been few and limited attempts to determine the long-term stability of the PSR 1257+12 system. Using the resonance overlap criterion and direct integrations, Rasio et al.

¹ e-mail: k.gozdziewski@astr1.uni.torun.pl

² e-mail: maciej@gps.caltech.edu

³ e-mail: alex@astro.psu.edu

(1992), Malhotra et al. (1992) and Malhotra (1993b) have found that the system disrupts on 10^5 yr timescale if the masses exceed about 2–3 masses of Jupiter. Also Malhotra et al. (1992) and Malhotra (1993a) have estimated that if the masses were about $20 - 40 M_{\oplus}$ then the system would be locked in the exact 3:2 resonances which would lead to the TOA signal very different from what is actually observed. In this paper, we investigate the stability of the PSR 1257+12 system in the Gyr-scale. We also perform a dynamical comparison of the PSR 1257+12 system to the inner Solar System (ISS) as the dynamics of the ISS is mostly driven by interactions between the telluric planets and is basically decoupled from the dynamics of the outer Solar System (Laskar 1994, 1997). Finally, we carry out a preliminary analysis of the stability of the orbits of massless particles (e.g. dust particles or Kuiper belt type objects) to determine the zones where such particles could survive and possibly be detected.

2. NUMERICAL SETUP

The stability analysis performed in this paper has mostly numerical character and is understood in terms of the maximal Lyapunov Characteristic Number (LCN). Hence we treat the quasi-periodic orbital motions ($LCN \approx 0$) as stable and the chaotic ones ($LCN > 0$) as unstable. In order to resolve the character of the orbits efficiently, we use the so-called fast indicator MEGNO (Mean Exponential Growth factor of Nearby Orbits, Cincotta & Simó 2000). The MEGNO is directly related to the LCN through the linear relation $\langle Y \rangle = at + b$. For quasi-periodic motions $a \approx 0$ and $b \approx 2$ while for chaotic solutions $a \approx (\lambda/2)$ and $b \approx 0$ where λ is the LCN of the orbit. However, there is no general relation between the magnitude of the LCN and the macroscopic changes of the orbital elements (e.g., Murison et al. 1994; Michtchenko & Ferraz-Mello 2001). Even if the LCN is large, the system can stay bounded for a very long time. More insight into the relation of the degree of the irregularity of motion and the macroscopic changes of the orbits one can obtain with the FFT techniques (Michtchenko & Ferraz-Mello 2001) and its refined variant, the Modified Fourier Transform (MFT) developed by Laskar (1993). The MFT makes it possible to resolve the fundamental frequencies in a planetary system and to determine their diffusion rates (Robutel & Laskar 2001). In our tests, we use the MFT to verify the MEGNO integrations for massless particles (Section 4) and to identify the mean motion resonances (MMRs). During the computations of MEGNO, for every planet $k = A, B, C$, and also for massless particles ($k = 0$) the complex functions $f_k(t_i) = a_k \exp(i\lambda_k(t_i))$, are computed at discrete times t_i , where $t_{i+1} - t_i \approx 10$ days, over the time $2T$ between $13,000 P_C$ and $64,000 P_C$ (where P_C is the orbital period of the outermost planet C). Here, a_k denotes the semi-major axis of the relevant planet and λ_k is its mean longitude. In general, for a quasi-periodic solution of a planetary system, the frequency corresponding to the largest amplitude, a_k^0 , is one of the fundamental frequencies of motion, called the proper mean motion, n_k (Robutel & Laskar 2001). The 2-body MMRs can be identified through the condition $q\mathbf{v}_i - p\mathbf{v}_j \approx 0$, $i \neq j = A, B, C, 0$, where $p, q > 0$ are prime integers. The MFT code gives us the rates $\mathbf{v}_i/\mathbf{v}_j \approx p/q$ and then p and q are found by the continued fraction algorithm. Such resonances will be labeled as $P_1q : P_2p$ where P_1 and P_2 denote the bodies involved in the resonance. In this work we use the code which merges the MFT and MEGNO methods. It incorporates the MFT code which has been kindly

provided by David Nesvorný⁴.

If a planetary system is strongly interacting, MEGNO enables us to detect chaotic behavior typically over only $10^3 - 10^4$ orbital periods of the outermost planet. This feature is vital for examining large sets of the initial conditions (see e.g., Goździewski et al. 2001; Goździewski & Maciejewski 2003). However, due to very small masses in the PSR 1257+12 system, the mutual perturbations between the planets are very weak. In order to resolve the character of such orbits, much longer integration times are required. We have determined that the general purpose integrators (like the Bulirsh-Stoer-Gragg, BSG) used to compute MEGNO are not efficient enough. Therefore, we have developed a symplectic scheme of computing MEGNO based on the idea of Mikkola & Innanen (1999) (see also Goździewski (2003) and Cincotta et al. (2003)). Instead of directly solving the variational equations of the perturbed Kepler problem, one can differentiate the symplectic leap-frog scheme (Wisdom & Holman 1991) and compute the variations (and MEGNO) using the obtained symplectic tangent map. To use such a technique, a system of canonical variables is required. In these variables, the planetary problem can be divided into integrable Keplerian motions and a perturbation which is integrable in the absence of the Keplerian part (usually it depends only on the coordinates). Our MEGNO code works internally in the Poincaré coordinates (Laskar & Robutel 1995). As the integrator core, the second-(LR2) and third- (LR3) order schemes by Laskar & Robutel (2001) are used. These integrators are much faster than the BSG algorithm. We can efficiently perform intensive computations of MEGNO ($\approx 10^4$ points per stability map) for $\approx 10^6 P_C$, keeping the fractional error of the total energy and the angular momentum below 10^{-10} when the 4 d step (for the LR3 integrator) is used. The tangent map approach is particularly suitable for the pulsar system due to typically small eccentricities of the investigated configurations. The method will be described in detail elsewhere (Breiter and Goździewski).

However, one should be aware that even with such an extended integration time-scale, in general we can only detect the strongest chaotic behavior originating mostly from the mean motion resonances between the planets. Investigations of subtle chaos originating in the secular system would require much longer integration times, of the order of thousands of secular periods. Because these periods are in the range $10^3 - 10^5$ yr (see Sect. 3) or longer, the total integration time should be counted in tens of Myr. In such a case, due to the computational limitations, direct approach applied in this paper is no longer practically possible.

In the numerical experiments, we use the initial condition given in Table 1. It represents one of the two orbital configurations obtained by Konacki & Wolszczan (2003) transformed to the classical astrocentric elements. In some of the experiments these elements have been transformed to the canonical heliocentric elements inferred from the Poincaré coordinates. In the second orbital configuration, the inclinations are such that $i_{B,C} \rightarrow 180^\circ - i_{B,C}$. We assume that i_A obeys the same rule in that solution. It follows that both these solutions are dynamically equivalent and this reflects the fact that using the secular theory as the model of TOA measurements we are still not able to determine the absolute direction of the angular momentum vector. The TOA residuals exclude opposite di-

⁴ www.boulder.swri.edu/~davidn/fmft/

rections of the outermost orbits (Konacki & Wolszczan 2003) hence the orbits are either prograde or retrograde.

3. STABILITY OF THE PSR 1257+12 PLANETARY SYSTEM

We computed the MEGNO signature of the PSR 1257+12 system over a few Myr ($5 \cdot 10^6 P_C$). This test was repeated for many different, randomly selected initial variational vectors. The results of a few of the runs are shown in Figs 1fe. Both the regular evolution of MEGNO, $Y(t)$, as well as the quick convergence of its mean value, $\langle Y \rangle(t)$, to 2, indicate that the system is very close to a quasi-periodic motion. Let us note, that our preliminary computations of MEGNO with the BSG integrator revealed a very slow divergence of MEGNO after $0.5 \cdot 10^6 P_C$ from the theoretical value of 2. It can be explained by an accumulation of the numerical errors because this effect is absent in much longer runs employing the symplectic code. Even if such a weak instability were to be understood in terms of the chaotic behavior, it would correspond to an extremely long Lyapunov time, $T_L = 1/\lambda$, comparable to 10^9 yr (estimated through the fit of the relation $\langle Y \rangle = (\lambda/2)t + b$ over $t \simeq 3.5 \cdot 10^6$ yr).

In Fig. 1, we present the time-evolution of the canonical heliocentric elements. Clearly, the motion of the planets B and C is tightly coupled. This is illustrated in panels b and c which show the variations of the eccentricities and inclinations. Fig. 1d demonstrates the presence of a deep, so-called secular apsidal resonance (SAR), described by the argument $\theta = \varpi_B - \varpi_C$ (where $\varpi = \omega + \Omega$ is the longitude of periastron; Ω and ω are the longitude of ascending node and the argument of periastron of the planet, respectively), with a small semi-amplitude of the librations, $\simeq 50^\circ$, and the apsides on average anti-aligned. In the discovery paper, Wolszczan & Frail (1992) noticed the anti-alignment of the lines of apsides while Rasio et al. (1992) and Malhotra et al. (1992) performed first theoretical explorations of the resonance in the framework of the Laplace-Lagrange theory.

The SAR was recently found in many extrasolar systems discovered by the RV measurements. It is widely believed that the SAR, as the orbital state of multi-planetary systems involving Jupiter-size planets, is crucial for maintaining their long term stability (for an overview see, Ji et al. 2003). However in certain cases, the SAR should be understood as a typical feature of a planetary system when the secular angle θ oscillates about 0° or 180° . In particular, this concerns the pulsar system: an inspection of Table 3 shows that the proper frequencies of the pericenter motion, g_p , are not related through any simple linear combination fulfilling the usual resonance rules. Lee & Peale (2003) and Michtchenko & Malhotra (2004) show that the orbital configurations of two planets are generically stable if the system is far from strong mean motion resonances and collision zones, i.e., when the assumptions of the averaging theorem are fulfilled. In such a case, the secular character of the system depends on the variations of the angle θ . Three different modes of its motion are possible: circulation, oscillations around 0° or 180° and oscillations about 0° in the regime of large eccentricities. The first two modes are known from the classical Laplace-Lagrange linear secular theory (Murray & Dermott 2000) while the third one was discovered by the cited authors. The third mode corresponds to the true, non-linear resonance and the secular system may be unstable in its neighborhood. It should be noted that for the two first modes there is no zero-frequency separatrix between the circulation and oscillation regimes. In this sense, such a SAR is not a true resonance.

Due to a very small mass of the planet A, the pulsar system may be approximated by a 3-body model with equal planetary masses, small eccentricities and inclinations. In such a case, Pauwels (1983) showed that, at least in the linear approximation, the SAR regime covers almost the entire phase space of the secular planetary system, the occurrence of a SAR is almost a certainty and the system is stable. This could explain the stability of the pulsar system. However, some of its specific dynamical features break the assumptions of the secular model. Namely, the proximity of the system to the first-order 3:2 MMR and other mean motion resonances. In order to estimate the influence of the near 3:2 MMR on the secular solution, we integrated the system over 10 Myr sampling the orbital elements every 100 yr. Subsequently, the MFT was applied to analyze the complex signals $e_p \exp(i\varpi_p)$ and $\sin(i_p/2) \exp(i\Omega_p)$ derived from the heliocentric canonical elements. In this way, we can obtain an estimate of the precessional frequencies of the periastrons, g_p , and the nodal lines, s_p . These frequencies, together with the proper mean motions, n_p , compose the set of fundamental frequencies of the pulsar system. Their values and the corresponding periods are given in Table 3. The periastron frequencies, measured in arcsec/yr, are $\simeq 197.742$, $\simeq 43.881$ and $\simeq 13.157$. The first one is substantially different from its analytical approximation (in terms of the Laplace-Lagrange theory). This will lead to a fast discrepancy between the analytical and numerical solutions. Clearly, the classical secular theory has to be modified in order to account for the effects of the near 3:2 MMR. Such a theory has been already developed by Malhotra et al. (1989) for the satellites of Uranus. It can also be applied to the PSR 1257+12 system however it is somewhat beyond the scope of this paper.

Using the symplectic integrator WHM (Wisdom & Holman 1991) from the SWIFT package (Levison & Duncan 1994) as well as the LR2 integrator, we also performed a few long term, 1 Gyr, integrations of the PSR 1257+12 system. In the first case, the time step equal to 1 d resulted in the fractional error of the integrals of the angular momentum and the total energy at the level of $\simeq 10^{-10}$. The LR2 algorithm with the 4-day integration step resulted in even higher accuracy. During the 1 Gyr interval, no signs of instability are observed. We have not detected any secular changes of the semi-major axes, eccentricities and inclinations. Their values stay within the limits shown in Fig. 1 and the SAR persists with an unchanged amplitude of the librations (Fig. 2a) over 1 Gyr.

Lest us note that from the 1 Gyr integrations it follows that the orbital elements of the innermost planet A vary in a regular way (Fig. 1). We can also observe a time evolution of the argument $\theta_1 = \varpi_A - \varpi_B$ as a semi-regular sequence of rotations alternating with irregular "librations" about 180° . This effect is preserved over the entire period of 1 Gyr (see Fig. 2c,d) and may indicate that the orbit crosses the separatrix of a resonance. This is illustrated in Figs 2c,d which show the eccentricity of the planet A (multiplied by 10,000), e_A , plotted together with the argument θ_1 . Clearly, there is a correlation between the librations of θ_1 and small values of e_A . We also show $e_C(\theta)$ and $e_A(\theta_1)$ collected over the 1 Gyr integration (Fig. 2e,f). The first case represents a trajectory in the resonant island of the SAR whereas there is no clear sign of librations in the $e_A(\theta_1)$ plot. In fact, this effect is only geometrical in nature and can be explained by estimating the secular frequencies of the system using the well known Lagrange-Laplace theory. If the MMRs are absent and the disturbing function is expanded up to the first order in the masses

and to the second order in the eccentricities and inclinations, the equations of the secular motion are integrable. Their solution, relative to the eccentricities and the longitudes of periastron, is given in terms of the so called eccentricity vectors, $(h, k) = (e \sin \varpi, e \cos \varpi)$, by (Murray & Dermott 2000)

$$h_j(t) = \sum_i e_{j,i} \sin(g_i t + \beta_i)$$

$$k_j(t) = \sum_i e_{j,i} \cos(g_i t + \beta_i),$$

for every planet $j = A, B, C$. The constant amplitudes $e_{j,i}$ and secular frequencies g_i are the eigenvectors and eigenvalues of a matrix with coefficients given explicitly in terms of the masses and constant semi-major axes of the planets. The scaling factors for the eigenvectors $e_{i,j}$ and the phases β_i are determined by the initial condition. Geometrically, the time evolution of every eccentricity vector can be described as a superposition of the eigenmodes corresponding to g_i (Malhotra 1993b). The parameters obtained for the PSR 1257+12 system are given in Table 2. They are consistent with the results of Malhotra (1993a) and Rasio et al. (1992) who analyzed the PSR 1257+12 system involving the two larger companions. They found that the secular evolution of the eccentricity vectors of the two outer planets is almost entirely driven by the eigenstate corresponding to g_1 . Since we have $e_{B,1} \simeq -e_{C,1}$ and the other components of $e_{j,i}$ are much smaller and almost equal, it follows that $\omega_B \simeq \omega_C + 180^\circ$, which corresponds to the SAR of the planets B and C. For the planet A, the eccentricity vector is a superposition of all the three eigenmodes with the leading second and third mode having comparable amplitudes. It appears that using the secular approximation, we can explain the semi-librations of θ_1 . The minima of e_A occur when the modes corresponding to the frequencies g_2 and g_3 are in anti-phase. Because the amplitudes $e_{A,2}$ and $e_{A,3}$ have the same sign and similar magnitudes while $e_{A,1}$ has a much smaller magnitude, the following condition has to be satisfied to grant a minimum of e_A

$$(g_2 t + \beta_2) - (g_3 t + \beta_3) \simeq 180^\circ.$$

Since $\beta_2 - \beta_3 \simeq -180^\circ$ (see Table 2), we have $(g_2 - g_3)t = 360^\circ$ and the period of anti-alignment is $P_{23} = 360^\circ/(g_2 - g_3) \simeq 43,000$ yr. Curiously, from the relation between g_i , $g_1 - 7(g_2 - g_3) \simeq 0.001^\circ/\text{yr}$, it follows that this period is almost commensurate with P_1 (where $P_1 = 360^\circ/g_1$).

Near the moment of anti-alignment, the eccentricity of the planet A, e_A , is driven mostly by the g_1 -mode that is in anti-phase with the eccentricity vector for e_B . This leads to the quasi-librations seen in Fig. 2 as they repeat with the same period as the variations of e_A , P_{23} .

3.1. Comparison to the inner Solar System

The results of the 1 Gyr integration, expressed in the canonical heliocentric elements, enable us to analyze the time-evolution of the so-called Angular Momentum Deficit (AMD, Laskar 1997):

$$C = \sum_{p=A,B,C} \frac{m_p m_\star}{m_p + m_\star} \sqrt{\mu_p a_p} (1 - \sqrt{1 - e_p^2} \cos i_p),$$

where $\mu_p = G(m_p + m_\star)$, G is the gravitational constant, a_p, e_p, i_p is the semi-major axis, eccentricity and inclination of a planet relative to the invariant plane and m_\star is the mass of the central body. The AMD indicates the deviation of planetary orbits from a stable circular and coplanar motion for which

$C = 0$. This quantity is preserved by the averaged equations of motion (Laskar 1997) and its stability provides the stability of the secular system in the absence of short-period resonances. The AMD can be understood as the amplitude of the irregularity present in the averaged system. Large values of AMD lead to a chaotic motion and for a certain critical value to a crossing of the orbits and the disruption of a planetary system (Laskar 1997, 2000; Michtchenko & Ferraz-Mello 2001).

The PSR 1257+12 system is close to the 3:2 commensurability. Its critical argument circulates but it does not mean that the time-averaged effects of the near-resonance vanish (Malhotra et al. 1989; Malhotra 1993a). Hence, the applicability of the AMD signature in the studies of the stability in the real, unaveraged system can be problematic. Instead, the integral obtained by averaging the quasi-resonant system should be applied (Michtchenko & Ferraz-Mello 2001). Nevertheless, we have decided to calculate the AMD and to examine its behavior in order to compare the results with those obtained for the Solar system (which contains two planets close to 5:2 MMR, see e.g., Ito & Tanikawa 2002). The time evolution of AMD in the pulsar system is shown in Fig. 2. The AMD stays well bounded and very regular. There is very little exchange of the AMD between the innermost planet A and the pair of the bigger companions B and C. It suggests that the motion of the planet A is decoupled from the dynamics of the planets B and C in the long-term scale. This situation is qualitatively different from the inner Solar system (ISS). The AMD of the ISS is not strictly preserved due to the perturbations of Jupiter and Saturn, nevertheless it can be considered roughly constant (Laskar 1997; Ito & Tanikawa 2002). Ito & Tanikawa (2002) published the results of 5 Gyr integrations of the ISS which reveal rapid AMD variations of Mercury. They are much larger than the changes of AMD for the Venus-Earth pair. The variations of the AMD of Venus, Earth and Mars are also irregular and substantial. In fact, the ISS is chaotic having the Lyapunov time of about 5 Myr (Laskar 1994). Laskar (1994) found that this chaos is physically significant as it can lead to the ejection of Mercury from the inner ISS during a few Gyr. However, the source of chaos in the ISS is still not well understood (Lecar et al. 2001). In this sense, the character of the motion of the PSR 1257+12 system is quite different. The evolution of its AMD is very regular in spite of smaller distances, larger masses and thus stronger mutual interactions between the planets. Unlike Mercury's, the AMD of the planet A is negligible when compared to the AMD of the B-C pair as it contributes only about 1/1000 of the total value. On the other hand, the orbital coupling of the pairs B-C and Venus-Earth (Ito & Tanikawa 2002) is a similar feature of the inner Solar and PSR 1257+12 systems although it has a different nature. The long term integrations by Ito & Tanikawa (2002) revealed an anti-correlation between the changes of the orbital energies of Venus and Earth and, simultaneously, a correlation between the changes of their orbital angular momenta and the eccentricities. These effects can be explained through the influence of the Jovian planets. Hence their dynamical source is external for the coupled planets while the coupling of the B-C pair in the PSR 1257+12 system is provided by the anti-aligned SAR. Finally, the chaotic orbital evolution of the ISS may significantly depend on the weak coupling with the outer planets. An equivalent effect is obviously absent in the PSR 1257+12 system.

3.2. Dynamical environment of the PSR 1257+12 planetary system

In the next set of experiments, we look at the initial condition in a global manner in order to find out whether the current state of the system is robust to the changes of the formal initial condition (IC). However, thanks to a very precise determination of the initial condition such changes, if considered consistent with the TOA measurements, are very limited. For example, the formal 1σ error of the semi-major axes inferred from the parameter x^0 (Konacki & Wolszczan 2003) is at the level of 10^{-6} AU! Nevertheless, the localization of the IC in the phase space (e.g. its proximity to unstable regions) is critical to verify its character. The examination of one isolated IC does not provide a definitive answer to the question of stability.

3.2.1. Mean motion resonances

We computed one-dimensional scans of MEGNO, $\langle Y \rangle$, by changing the semi-major axis of one planet and keeping the other orbital parameters fixed at the values given in Table 1. The results of this experiment are illustrated in Fig. 3. The MEGNO scans were computed with the resolution of $\simeq 5 \cdot 10^{-6}$ AU and 10^{-6} AU for close-up scans. They reveal a large number of spikes, some of them very close to the nominal positions of the planets marked with the large filled dots. Most of these spikes can be identified as 2-body MMRs between the planets. Currently, the IC is well separated from low-order MMRs. But some unstable high-order MMRs appear close to the nominal IC. The most relevant ones seem to be C31:B21 MMR (i.e. between the planets B and C, see the bottom panel in Fig. 3) and C53:B36 MMR (shown in the scan for the planet B). Also the planet A is close to B29:A11 MMR. Yet, such resonances are extremely narrow. Their widths can be roughly estimated as less than $5 \cdot 10^{-6}$ AU what follows from their shapes and the resolution of the MEGNO scans. It is unlikely that they can affect the regular motion of the system at its nominal position. However, altering the semi-major axis of the planets by small shifts, $\simeq 5 \cdot 10^{-5}$ AU, would push the system into these unstable regimes. In order to demonstrate it, we calculated MEGNO for a configuration corresponding to C31:B21 MMR (see the right column of Fig. 4). This resonance is the inclination-type MMR (according to the terminology by Peale 1976). Clearly, its critical argument $\sigma = 31\lambda_C - 21\lambda_B - 10\Omega_B$ exhibits a sequence of alternating librations and circulation giving rise to the unstable behavior. Let us note, that the chaos is formally extremely strong. The Lyapunov time, estimated by the linear fit to the MEGNO, is only about 3000 yr (see Fig. 4a).

The 2-body MMRs cannot explain all the peaks of MEGNO present in the scans. Some of them seem to be related to the 3-body resonances involving all three planets. The importance of 3-body MMRs was studied by Nesvorný & Morbidelli (1998); Morbidelli & Nesvorný (1999), Murray et al. (1998) and Murray & Holman (1999). They found that weak 3-body MMRs can strongly influence asteroidal motion and explain the short Lyapunov times which cannot be understood if only 2-body MMRs of high-order are considered. Murray & Holman (1999) proved that the chaotic behavior of the Outer Solar system is governed by the overlapping 3-body MMRs involving Jupiter, Saturn, and Uranus. It is obviously interesting to verify if some of the instabilities visible in the a -scans can be related to such 3-body resonances.

A 3-body resonance can be defined by the following condi-

tion (Nesvorný & Morbidelli 1998):

$$i_A \dot{\lambda}_A + i_B \dot{\lambda}_B + i_C \dot{\lambda}_C \simeq 0,$$

where $\dot{\lambda}_p$ is the mean motion of the given planet. A critical argument of such resonance is a linear combination of the longitudes, arguments of pericenters and nodal longitudes:

$$\sigma_{i_A:i_B:i_C} = i_A \lambda_A + i_B \lambda_B + i_C \lambda_C + p_A \varpi_A + p_B \varpi_B + p_C \varpi_C + q_A \Omega_A + q_B \Omega_B + q_C \Omega_C$$

whose integer coefficients i_p, p_p, q_p fulfill the d'Alambert rule $\sum_{p=A,B,C} (i_p + p_p + q_p) = 0$ and the usual requirement of rotational symmetry. Due to the small ratios of the secular frequencies to the mean motions in the PSR 1257+12 system, $\simeq 10^{-5}$, the resonance condition may be approximated by $i_A n_A + i_B n_B + i_C n_C \simeq 0$. For example, one of the MEGNO peaks for $a_C = 0.46601$ AU, can be explained as the combination of the proper mean motions $3n_A - 14n_B + 9n_C \simeq 0.01^\circ/\text{yr}$. Hence it corresponds to the 3-body MMR 3:-14:9. It is separated from the nominal position of the planet C by only $\simeq 3 \cdot 10^{-5}$ AU which is at the 3σ error level of a_C . The time evolution of the critical argument, $\sigma_{3:-14:9}$, shown in the left column of Fig. 4, confirms the slow changes of this angle as well as a presence of quasi-librations alternating with circulations. This indicates a chaotic evolution. The MEGNO computed for the corresponding initial condition does not grow fast, at least over a few Myr used in this test. This means that the chaos is moderate. Nevertheless, the long term stability of the system (likely, the chaos would affect mostly the motion of the planet A) could be confirmed only by direct numerical integrations. Our 1 Gyr integrations for the ICs of the two MMRs near the planet C do not reveal any secular changes of the elements. Likely, in order to properly investigate subtle effects of these resonances and their influence on the system, a refined model of the motion should be used. Such model should incorporate the effects of general relativity, a possible error in the pulsar mass and other factors, like the dependence on the observationally unconstrained orbital elements of the planet A.

Other low-order 3-body resonances that can be identified in the Fig. 3 are 1:-2:1, 1:-4:2, -2:10:7 (almost overlapping with B71:A27), 3:-16:12, 1:-6:5 (see the a_A -scan). Finally, also an overlapping of 2-body MMRs is possible. One such example is marked in the a_B -scan where in the neighborhood of the 3:2 MMR, a sharp peak of MEGNO at the simultaneous position of B60:A23 and C76:B51 MMRs is present. All these MMRs are very narrow since the width of 3-body MMRs is proportional to the masses in the second order and these 2-body MMRs are of high order. They are relatively distant from the nominal positions of the planets thus it is unlikely that they can affect the motion of the system.

Finally, Fig. 4 shows the effect of varying the assumed mass of the neutron star on the determination of the semi-major axis of the outermost planet and the localization of the resonances. Obviously, the sequence of MMRs does not change. A different mass of the pulsar can lead to a substantial shift of the initial semi-major axis (in our case, a_C) and the weak unstable resonances, like the C31:B21 MMR, may end up much closer to the nominal positions of the planets (for smaller than canonical mass of the parent star, $M_{\text{psr}} = 1.4M_\odot$).

3.2.2. Stability in the (a_p, e_p) - and (e_B, e_C) -planes

The results of the 2-dimensional MEGNO analysis are shown in Fig. 6. In these maps we analyze the influence of

the initial eccentricities of the planets on their motion. We used the initial conditions from Table 1 and changed those elements that correspond to the coordinates in the stability maps. Due to a lower resolution (400 points in the semi-major axis range), some features present in the one-dimensional scans are not so clearly visible. Nevertheless, in the (a_B, e_B) -plane (the middle panel), the thin strips of the MMRs can be easily identified. These maps additionally reveal the width of the strongest MMRs (like C3:B2, C13:B9 and C10:B7) and the border of the global instability. These stability maps confirm that the nominal positions of the two bigger planets, marked with filled circles, are far from strong instabilities of the motion. Also in the (e_B, e_C) -plane, the nominal IC lies in a wide stable region, far from zones of chaotic motion (see Fig. 7). The (a_A, e_A) -map for the planet A shows a dense net of narrow unstable regions, some of which are close to the nominal position of the planet. They have been already identified in the 1D scans for a_A . Let us note that similar maps were computed by Ferraz-Mello & Michtchenko (2002) for the planet B with their FFT fast indicator. Their results are generally consistent with ours even though they used a different initial condition of the pulsar system.

During the MEGNO integrations we have also computed the maximum value of the SAR argument $\theta = \bar{\omega}_B - \bar{\omega}_C$ with respect to the libration center of 180° . It enables us to estimate the semi-amplitude of librations and the extent of the SAR in the space of the scanned orbital parameters. The result of such an experiment conducted in the (a_B, e_B) plane are shown in Fig. 8. It uncovers an extended zone of the SAR with the smallest semi-amplitude of θ in the vicinity of the nominal initial condition of the PSR 1257+12 system. The near 3:2 MMR is also clearly present in this map.

3.2.3. Limits on the unconstrained parameters of planet A

So far, after Konacki & Wolszczan (2003), we were using the average inclination of the orbits of the planets B and C as the orbital inclination of the planet A. However, we can try to verify whether the dynamics can provide any limits on the inclination and hence mass of the innermost planet A. To this end, we computed MEGNO for the inclination of the planet A in the range $[30^\circ, 70^\circ]$ and the position of its nodal line in the range $[-90^\circ : 90^\circ]$, with the resolution of 1° in both coordinates. Thus we varied both the mass (to preserve $m_A \sin i_A$ determined from the TOAs) as well as the relative inclination of the planet A to the orbital planes of B and C. The result of this experiment is shown in Fig. 9. The MEGNO scan (the left panel of Fig. 9) reveals a well defined stable region. The assumed position of the planet A is in the center of this zone. To obtain this picture, an extended integration time span of $10^6 P_C$ was used. This choice was dictated by the analysis of a few orbits of A which are substantially inclined to the orbital planes of B and C. An example corresponding to the initial $\Omega_A = -75^\circ$ (thus located in the unstable region) is shown in Fig. 10. For the integration time up to about 0.5 Myr ($\simeq 5 \cdot 10^5 P_C$) MEGNO stays close to 2 but then it suddenly grows, indicating chaotic behavior. To explain its source, we computed the eccentricity, inclination i_A^{rel} and the argument of pericenter, g_A , of the planet A relative to the invariant plane. Evolution of these elements is shown in Fig. 10. Clearly, both e_A and i_A^{rel} exhibit long-term, large amplitude oscillations which are exactly in an anti-phase. The period of these oscillation is relatively very long, of the order of 10^4 yr. Simultaneously, g_A temporarily librates about 90°

or 270° . These librations indicate that the pericenter precession of A stops. Such features are typical for the well known Kozai resonance (Kozai 1962) found for highly inclined asteroids in the Solar system. The argument of pericenter g_A can be treated as the critical argument of this resonance. Because librations are followed by circulations of the critical argument, the orbit crosses the separatrix which explains why the motion eventually becomes chaotic.

The effects of the Kozai resonance are illustrated in the right panel of the e_A^{max} -map (the maximal eccentricity attained by the planet A during the integration time) in Fig. 9. The sharply ending zone of moderate eccentricities is narrower than the stability region. We should be aware that in the transient areas the integration time could still be too short to detect the irregular motion. Note that around the border of the stable zone, e_A can be as large as 0.6–0.8. This resonance puts significant limits on the position of the nodal line of the planet A as well as its relative inclination to the orbital planes of B and C. Assuming that the motion of all three planets is in the same direction, the nodal line of A cannot be separated by more than about $\pm 60^\circ$ from the nodes of B and C and the relative inclination should not exceed $\simeq 45^\circ$. Otherwise, the eccentricity of A would be excited to large values, > 0.7 over only 10^5 yr and for $e_A \simeq 0.8$ the orbits of A and B would cross or close encounters would become possible.

4. DYNAMICS OF MASSLESS PARTICLES

While investigating the dynamics of extrasolar planetary systems one can ask whether the minor bodies can survive in the gravitational environment of the giant primary bodies. These can be small telluric planets in the systems with Jupiter-like planets. We can ask the same question about asteroids, cometary bodies or dust particles in the PSR 1257+12 system. Because the motion of the planets appears to be strictly stable, we can consider a simplified, restricted model. In this model one assumes that a probe mass moves in a gravitational tug of the primaries but does not influence their motion. In the simplest case such a model is well known as the restricted, planar circular 3-body problem (Murray & Dermott 2000). This simplification helps us to explore the phase space of the planetary system with reasonable computational effort. In this model, the MEGNO indicator and the MFT are evaluated only for the probe mass. In the numerical experiments, we investigate the orbital stability of massless particles in a few regions of the orbital space: between the planets A and B (region I), B and C (region II) and beyond the planet C (region III).

In the first series of numerical tests, we vary the initial semi-major axis of the probe mass, a_0 , and its eccentricity, e_0 , while the initial inclination is constant, $i_0 = 50^\circ$. Thus the tested orbits are slightly inclined to both orbital planes of the planets B ($i_B = 53^\circ$) and C ($i_C = 47^\circ$). The angular variables of the massless particles are set to $\Omega_0 = \bar{\omega}_0 = M_0 = 0^\circ$. This way we essentially follow the remarkable work of Robutel & Laskar (2001) who investigated the short-term dynamics of massless particles in the Solar System using the MFT. These authors argue that the global picture of the motion in the restricted problem does not qualitatively depend on the initial phases of the test particle. The initial plane (a_0, e_0) is representative for the dynamics because it crosses all resonances. By changing the initial orbital phases of the massless particles, the width of the resonances may vary but their influence on the motion can still be detected.

In order to check the MEGNO signatures (e.g., to verify

whether the integration time is not too short), during the integrations, we compute the diffusion rate, $\sigma_0 = 1 - n^{(2)}/n^{(1)}$, where $n^{(1)}$ and $n^{(2)}$ are the mean motion frequencies obtained over the intervals $[0, T]$ and $[T, 2T]$, respectively, where T (which we will call the base period from hereafter) has been set accordingly to the investigated range of the semi-major axes. The close encounters with the planets are controlled. We assume that if the distance between the probe mass and a planet is less than the Hill radius, $r_H = [m_p/(3m_*)]^{(1/3)}a_p$, then the particle has collided with the planet or its motion become strongly chaotic.

Within this numerical setup, in the region II we have not detected any stable motions. The region I turns out to be a much more interesting one. The results are shown in the MEGNO and σ maps in Fig. 11 (left panels for the region I, middle and right panels for the region III). The integrations have been carried out for the total time, $2T$, of about 32,000 P_C . In both maps we can clearly recognize the planetary-crossing lines marked by large values of both indicators which correspond to strongly chaotic motions. These lines (white lines in Fig. 11) are the solutions to the equations $a_p(1 + e_p) = a_0(1 - e_0)$ for $a_0 > a_p$ and $a_p(1 - e_p) = a_0(1 + e_0)$ for $a_0 < a_p$ where a_p, e_p, a_0, e_0 denote the initial semi-major axis and the eccentricity of a planet and a test particle, respectively.

In this area and above the collision lines, the particles are scattered mostly by close-encounters and collisions with the planets A and B. Remarkably, a stable area exists under the crossing-lines for the planets A and B. It is divided by a number of MMRs with the planets. In order to verify this result, we have integrated the motion of 200 particles spread over $[0.19, 0.35]$ AU with the same resolution in the semi-major axis, a_0 , as in the 2D MEGNO test. These integrations were continued up to 15 Myr (here, we used the RMVS3 integrator from the SWIFT package). A resulting one dimensional scan of MEGNO over a_0 is shown in Fig. 12. In the regions classified with MEGNO as regular, the massless particles have mostly survived during the integration time while in the chaotic or close to chaotic areas, they have been quickly removed or collided with the planets (in this test the same criterion of 1 Hill radii for a collision event is used and in such a case we set $\log \sigma_0 = 1$). Some discrepancies are most likely related to the different integrators used in the experiment; the Bulirsh-Stoer integrator follows the orbits of massless particles much more accurately than the symplectic integrator. This experiment enables us also to independently estimate the proper MEGNO integration time and to "calibrate" the scale of the diffusion rate, σ_0 . Comparing the MEGNO and σ_0 -maps, we conclude that for $\log \sigma$ less than about $(-7) - (-8)$ the motion can be considered as regular (also compare the maps in the left column of Fig. 11). Let us note that both indicators are in an excellent accord and the diffusion rate calculated by the MFT algorithm seems to be even more sensitive to an unstable motion than the MEGNO is.

Using a similar numerical setup, we have investigated the region III. However, due to an extended range of the semi-major axes, we have divided it into two parts: the region IIIa between 0.5 AU and 0.97 AU and the region IIIb between 0.9 AU and 3.9 AU (a distance comparable to the radius of the Asteroid Belt in the Solar System). The maps of MEGNO and the diffusion rate, $\log \sigma$, in the (a_0, e_0) -plane for the region IIIa (obtained after the time $2T \simeq 32,000 P_C$), are shown in the middle column of Fig. 11 while the maps for the region IIIb ($2T \simeq 64,000 P_C$) are shown in the right column. For

the region IIIa, in both maps, we can clearly recognize the collision line with the outermost planet while the crossing line with the planet B is in the zone of strong chaos. A number of MMRs appear as narrow vertical strips. This test shows that for a moderately low initial eccentricity, e_0 , the stable zone is extended and begins just beyond the orbit of the planet C. Obviously, with a growing e_0 the border of the stable zone shifts toward a larger a_0 (at the distances of about 1 AU the zone of stability reaches $e_0 \simeq 0.5$). For the region IIIb ($a_0 \in [0.9, 3.9]$ AU), the results are shown in the right column of Fig. 11. For efficiency reasons, in this test the step in e_0 is 0.1 (the resolution in a_0 was left relatively high, at 0.005 AU). The collision lines are clearly present. Otherwise, this zone is mostly regular even for very large $e_0 > 0.5$. Similarly to the region IIIa, the scans reveal some extremely narrow unstable MMRs, most of them with the two outer planets.

Finally, we examined the stability of orbits inclined to the mean orbital plane of the system. In this experiment we tested the motion of particles in the region III. The results for the region IIIa are shown in Fig. 13 (a number of additional scans, not shown here, allow us to extrapolate the results obtained for this region to the region IIIb). In the first two experiments, we scanned the (a_0, e_0) space for the initial i_0 set to 75° and 87° , respectively. These inclinations, taken relative to the mean orbital plane of the PSR 1257+12 system, are comparable to the inclinations of the Kuiper belt objects in the Solar System. Again, the collision lines and the net of MMRs clearly appear in both the MEGNO and σ_0 scans which are shown in the left and the middle panels of Fig. 13. The zone of strong chaos covers the crossing zones with the planets B and C while the collision line with the planet A is much more narrow and separated by a quasi-regular area in which $\sigma_0 \simeq 10^{-6}$. Such an effect has been already observed by Robutel & Laskar (2001) — for higher inclination the close encounters with the planets are less frequent than for moderately small inclinations which explains the smaller extent of the strong chaos. Moreover, after sufficiently long time the massless bodies will be removed from above the collision lines, excluding cases when the probes are trapped within stable MMRs. In the next test illustrated in the right panel of Fig. 13, e_0 was set to 0 and the initial inclination i_0 was varied in the wide range $[10^\circ, 90^\circ]$. This experiments allow us to generalize the results of the previous scans. The stability of inclined particles is basically independent on the initial inclination, at least for moderately small eccentricities.

One should be aware that the results of the above analysis should be treated as preliminary ones. Our study is restricted both to the short-term dynamics and a small part of the possible volume of the parameter space. However, the timescale of the integrations is long enough to detect the most unstable regions in the phase space and to point out the regions where the particles can be long-term stable. Also in some chaotic regions the particles can still persist over a very long time but this can be verified only by direct integrations. Let us also note that in order to derive rigorous estimates of the *proper* mean motion frequencies one has to employ angle-action like coordinates, e.g., the Poincaré coordinates (Laskar & Robutel 1995) or the Jacobi coordinates. Our integrations for massless particles were carried out in the Keplerian, astrocentric coordinates and the osculating elements analyzed by MFT are inferred from these non-canonical coordinates. Due to very small masses involved, the effects caused by the use of non-canonical coordinates are negligible.

5. CONCLUSIONS

In this work we carry out numerical studies of the stability of the PSR 1257+12 system using the initial condition determined by Konacki & Wolszczan (2003). The long term integrations utilizing the symplectic integrators, extended over 1 Gyr, do not reveal any secular changes in the semi-major axes, eccentricities and inclinations of the planets. Using the notion of the Angular Momentum Deficit (AMD), we do not find any substantial exchange of the angular momentum between the innermost planet and the pair of the outer, bigger planets B and C. The AMD of the planet A is negligible when compared to the AMD of the B-C pair. This is very different from the case of the inner Solar System in which the variations of the AMD of Mercury are the most significant ones. The PSR 1257+12 system has the MEGNO signature typical for a strictly regular, quasi-periodic configuration. The two outer planets are close to the 3:2 mean motion resonance and are orbitally tightly coupled. The presence of the secular apsidal resonance is quite typical for such system as demonstrated by Pauwels (1983) and recently by Lee & Peale (2003) and Michtchenko & Malhotra (2004). The semi-amplitude of the critical argument is about 50° and it persists in a wide range of the orbital initial parameters. The SAR in the PSR 1257+12 system is yet another such case among extrasolar planetary systems (Ji et al. 2003).

The neighborhood of the nominal initial condition is investigated by calculating the MEGNO signature in a few representative regimes of the semi-major axes and eccentricities of the planets. These stability maps reveal that the nominal initial condition is located in an extended stable zone, relatively far from any strong instabilities of the motion. However, numerous weak mean motion resonances can be found in close proximity to the nominal positions of the planets. These are both 2-body resonances between the planets (like the 31:21 MMR between B and C) and 3-body resonances, among which the 3:-9:14 MMR seems to be the most relevant one. Their potential influence on the motion could be investigated if the initial condition of the system was refined using a more accurate model of the dynamics, possibly including relativistic effects. However, it would most likely require much more precise TOA measurements than currently available.

These factors allows us to state that the PSR 1257+12 system is orbitally stable over the Gyr time scale. In our experiments, there are no signs of a potential instability except for

a very slow divergence of the MEGNO in few of the tests. This divergence of MEGNO corresponds to the Lyapunov time of about $\simeq 1$ Gyr. We believe that it has only a numerical character. We are aware that an alternative analytical study of the PSR 1257+12 dynamics is possible (also thanks to the accurate determination of the initial condition). Such an approach has been proposed in Malhotra et al. (1989) and Malhotra (1993a). Our numerical investigations can certainly be treated as a complement to any future analytical studies of the system.

Using the MEGNO analysis, we found dynamical limits on the unconstrained elements of the planet A. Due to the destabilizing effect of the Kozai resonance, the nodal line of this planet cannot be separated by more than about $\pm 60^\circ$ from the nodes of B and C. Otherwise, the eccentricity of A would be excited to large values permitting close encounters or collisions with the planet B. It constitutes a strong dynamical argument that the orbital plane of the planet A indeed coincides with the mean orbital plane of the system.

Finally, using the MEGNO and the MFT, we investigate the dynamics of massless particles in the PSR 1257+12 system in the framework of the restricted model. In the numerical experiments, we find a stable zone between the planets A and B extending for initially small eccentricities from 0.19 AU to 0.25 AU from the pulsar. There are no stable areas between the planets B and C. Beyond the orbit of the planet C, the stable zone begins already outside of its orbit. We find that the massless particles can move on stable orbits under the condition that their initial eccentricities and semi-major axes are located under the collision lines with the planets. The dynamics of massless particles is basically independent on the their initial inclinations. Beyond 1 AU, the motion appears to be stable except for the areas of narrow MMRs with the planets B and C. It is an encouraging result supporting the search for possible small bodies contained in a dust or Kuiper belt type disk around the PSR 1257+12 .

6. ACKNOWLEDGMENTS

We are indebted to the anonymous referee for many invaluable suggestions and a detailed review which improved the manuscript. We thank Philippe Robutel for a discussion and helpful remarks. K. G. is supported by the Polish Committee for Scientific Research, Grant No. 2P03D 001 22. M. K. is a Michelson Postdoctoral Fellow.

REFERENCES

- Cincotta, P., Simó, C., & Giordano, C. 2003, Physica D, 182, 151
 Cincotta, P. M. & Simó, C. 2000, A&AS, 147, 205
 Ferraz-Mello, S. & Michtchenko, T. A. 2002, in Revista Mexicana de Astronomia y Astrofisica Conference Series, 7–10
 Goździewski, K. & Maciejewski, A. J. 2003, ApJ, 521
 Goździewski, K. 2003, A&A, 398, 315
 Goździewski, K., Bois, E., Maciejewski, A., & Kiseleva-Eggleton, L. 2001, A&A, 378, 569
 Ito, T. & Tanikawa, K. 2002, MNRAS, 336, 483
 Ji, J., Liu, L., Kinoshita, H., Zhou, J., Nakai, H., & Li, G. 2003, ApJ, 591, L57
 Konacki, M., Maciejewski, A. J., & Wolszczan, A. 1999, ApJ, 513, 471
 —. 2000, ApJ, 544, 921
 Konacki, M. & Wolszczan, A. 2003, ApJ, 591, L147
 Kozai, Y. 1962, AJ, 67, 591+
 Laskar, J. 1993, Celest. Mech. & Dyn. Astr., 56, 191
 —. 1994, A&A, 287, L9
 —. 1997, A&A, 317, L75
 —. 2000, Physical Review Letters, 84, 3240
 Laskar, J. & Robutel, P. 1995, Celest. Mech. & Dyn. Astr., 62, 193
 —. 2001, Celestial Mechanics and Dynamical Astronomy, 80, 39
 Laughlin, G. & Chambers, J. E. 2001, ApJ, 551, L109
 Lecar, M., Franklin, F. A., Holman, M. J., & Murray, N. J. 2001, ARA&A, 39, 581
 Lee, M. H. & Peale, S. J. 2003, ApJ, submitted
 Levison, H. F. & Duncan, M. J. 1994, Icarus, 108, 18
 Malhotra, R. 1993a, in ASP Conf. Ser. 36: Planets Around Pulsars, 89–106
 Malhotra, R. 1993b, ApJ, 407, 266
 Malhotra, R., Black, D., Eck, A., & Jackson, A. 1992, Nature, 356, 583
 Malhotra, R., Fox, K., Murray, C. D., & Nicholson, P. D. 1989, A&A, 221, 348
 Michtchenko, T. & Ferraz-Mello, S. 2001, ApJ, 122, 474
 Michtchenko, T. A. & Malhotra, R. 2004, Icarus, 168, 237
 Mikkola, S. & Innanen, K. 1999, Celestial Mechanics and Dynamical Astronomy, 74, 59
 Morbidelli, A. & Nesvorný, D. 1999, Icarus, 139, 295
 Murison, M. A., Lecar, M., & Franklin, F. A. 1994, AJ, 108, 2323
 Murray, C. D. & Dermott, S. F. 2000, Solar System Dynamics (Cambridge Univ. Press)
 Murray, N. & Holman, M. 1999, Science, 283, 1887
 Murray, N., Holman, M., & Potter, M. 1998, AJ, 116, 2583
 Nesvorný, D. & Morbidelli, A. 1998, AJ, 116, 3029

TABLE 1
ASTROCENTRIC OSCULATING ORBITAL ELEMENTS OF THE PLANETS IN PSR 1257+12 PLANETARY SYSTEM AT THE EPOCH MJD=49766.50.^a

Planet	Mass [M _⊕]	<i>a</i> [AU]	<i>e</i>	<i>i</i> [deg]	Ω [deg]	ω [deg]	M [deg]
A	0.019	0.18850	0.0000	50.00	0.00	0.0	14.25
B	4.250	0.35952	0.0186	53.00	0.00	250.4	5.41
C	3.873	0.46604	0.0252	47.00	3.26	108.3	3.66

^a The semi-major axis, *a*, the eccentricity, *e*, the inclination, *i*, the longitude of ascending node, Ω , the argument of periastron, ω , and the mean anomaly, *M*, of the planets in PSR 1257+12 planetary system at the epoch MJD=49766.50 are derived from the best-fit orbital parameters by Konacki & Wolszczan (2003). The mass of the central star is equal to 1.4 M_⊙.

Pauwels, T. 1983, Celestial Mechanics, 30, 229

Peale, S. J. 1976, ARA&A, 14, 215

—. 1993, AJ, 105, 1562

Rasio, F. A., Nicholson, P. D., Shapiro, S. L., & Teukolsky, S. A. 1992, Nature, 355, 325

Rivera, E. J. & Lissauer, J. J. 2001, ApJ, 402, 558

Robutel, P. & Laskar, J. 2001, Icarus, 152, 4

Wisdom, J. & Holman, M. 1991, AJ, 102, 1528

Wolszczan, A. 1994, Science, 264, 538

Wolszczan, A. & Frail, D. A. 1992, Nature, 355, 145

FIG. 1.— The orbital evolution of the nominal PSR 1257+12 system and its MEGNO signature. Panel (a) is for the semi-major axes. Panel (b) is for the orbital inclinations. Panel (c) is for the eccentricities. Panel (d) illustrates the secular apsidal resonance between the planets B and C. Panels (f) and (e) are for the time-evolution of MEGNO and its mean value, $\langle Y \rangle(t)$ (a few representative evolutions for different choices of the initial tangent vector are shown). The orbital evolution is given in terms of the heliocentric canonical elements related to the Poincaré coordinates.

FIG. 2.— The dynamics of the PSR 1257+12 system in the 1 Gyr integration. Panel (a) is for the critical argument of the secular apsidal resonance during 1 Gyr. Panel (b) is for the AMD. Panels (c) and (d) are for the argument $\theta_1 = \varpi_A - \varpi_B$. Panel (c) is for the first 0.2 Myr while panel (d) is for the end of the 1 Gyr period. The solid line in these plots denotes the eccentricity of the innermost planet multiplied by 10⁴. Panel (e) shows the SAR between the planets B and C in the space of $(\varpi_A - \varpi_B, e_C)$. The same plot for θ_1 and e_A is shown in panel (f). The orbital evolution is given in terms of the heliocentric canonical elements related to the Poincaré coordinates.

FIG. 3.— The dynamical environment of the PSR 1257+12 planets in the space of the semi-major axes. The plots are for the one-dimensional MEGNO scans along the semi-major axis of the planet A, B and C. All the other initial elements are fixed at their nominal values (see Table 1). The resolution of the scans is 5 · 10⁻⁶ AU and 10⁻⁶ AU (the later for the close-up scans for the planets A and C). Labels mark the positions of the MMRs between the planets: the upper plot and the second plot for the A-B pair the third, fourth and fifth panel from the top for the B-C pair. The upper plot is a magnification of the scan for the planet A, the bottom plot is a magnification of the scan for the planet C. Big dots mark the nominal positions of the planets.

FIG. 4.— The left column shows the evolution of the critical arguments of the MMRs close to the planet C (see the text for explanation). The panels in the right column are for MEGNO. The Lyapunov time about 3000 yr for the C31:B21 MMR is estimated through a linear fit to the MEGNO plot.

FIG. 5.— The MEGNO scan along a_C for different masses of the host star. The upper scan is for $m_\star = 0.95M_{\text{psr}}$ and the lower for $m_\star = 1.05M_{\text{psr}}$ where M_{psr} is the canonical mass of the pulsar, 1.4 M_⊙.

FIG. 6.— The MEGNO stability maps for the configuration given in Table 1. The left panel is for the (a_A, e_A) -plane. The middle panel is for the (a_B, e_B) -plane. The right panel is for the (a_C, e_C) -plane. The position of the nominal system is marked by the two intersecting lines.

FIG. 7.— The MEGNO stability map for the configuration given in Table 1. The scan is for the (e_B, e_C) -plane. The position of the nominal system is marked by the two intersecting lines.

FIG. 8.— The semi-amplitude θ^{\max} of the SAR in the (a_B, e_B) -plane. The position of the nominal system is marked by the two intersecting lines.

FIG. 9.— The stability map in the (i_A, Ω_A) -plane (the left panel) and the maximal eccentricity of the planet A attained during the integration time (the right panel). The resolution of the plot is 1° × 1°. The position of the nominal system is marked by the two intersecting lines.

FIG. 10.— Kozai resonance for a configuration corresponding to the initial $i_A = 50^\circ$ and $\Omega_A = -75^\circ$. Panel (a) shows the changes of the eccentricity and inclination of the planet A relative to the invariant plane of the system. Panel ga is for the argument of periastron, measured with respect to the invariant plane. Panel for $Y(t)$ shows the temporal variations of MEGNO and its mean value, $\langle Y \rangle$.

FIG. 11.— The stability maps for the massless particles in different regions of the PSR 1257+12 system. The left column is for the region II (between the planets A and B), the middle panel is for the region IIIa (beyond the planet C, up to 1 AU) and the right panel is for the region IIIb (up to 3.9 AU). The upper maps are for MEGNO, the bottom maps are for the diffusion rate $\log \sigma_0$. The resolution of the scans is 0.0008AU × 0.005, 0.0025AU × 0.005 and 0.005AU × 0.1, respectively. Collision lines with the planets are marked with white curves.

FIG. 12.— The MEGNO scan along the semi-major axis a_0 of the massless particles moving between the planet A and B (thick line) and their survival times over 15 Myr integrations (represented by thin vertical lines).

FIG. 13.— The stability maps for the massless particles moving in the region IIIa of the PSR 1257+12 system for different initial inclinations. The left column is for the initial inclination $i_0 = 75^\circ$, the middle column is for $i_0 = 87^\circ$. The right panels are for $e_0 = 0$ and $i_0 \in [10^\circ, 90^\circ]$. The upper maps are for MEGNO, the bottom maps are for the diffusion rate $\log \sigma_0$. The resolution of the scans is 0.0023AU × 0.04, 0.0019AU × 0.01, and 0.0019AU × 2°, respectively.

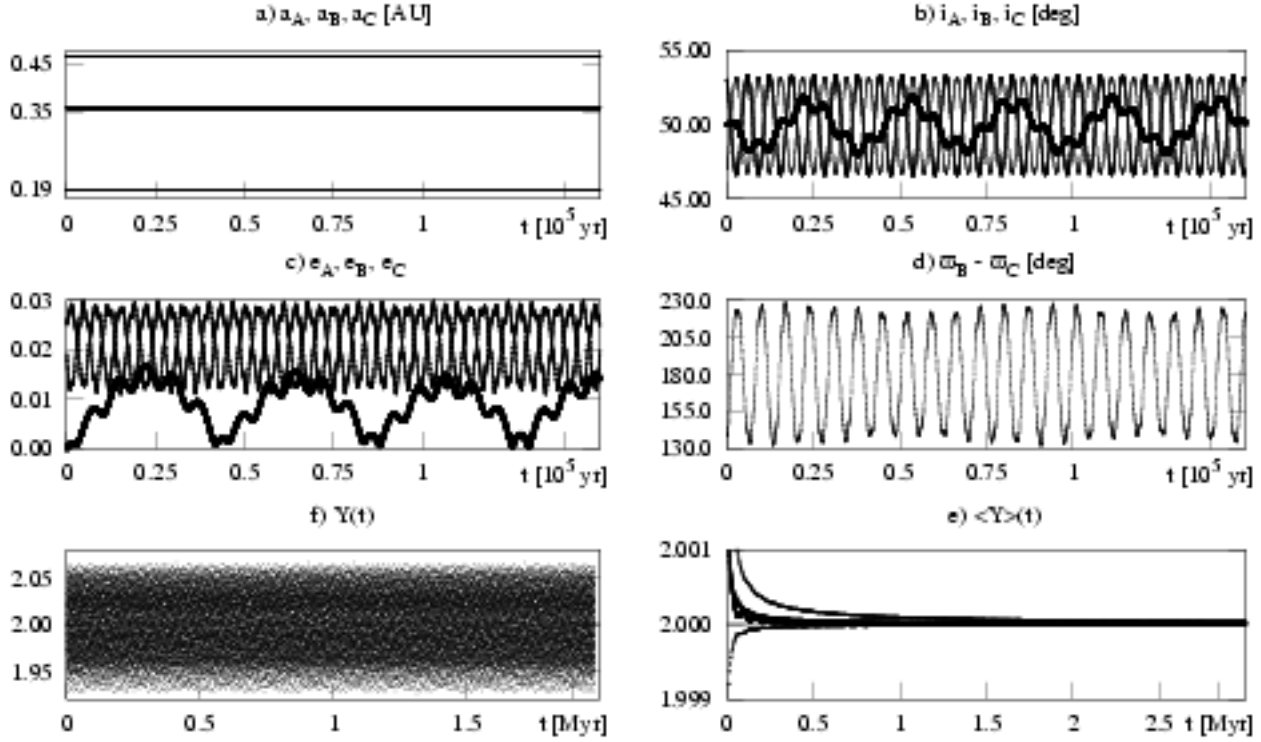


FIG. 1.—

TABLE 2
PARAMETERS FOR THE (h, k) SECULAR SOLUTION OBTAINED BY MEANS OF THE LAPLACE-LAGRANGE THEORY.
AMPLITUDES $e_{p,i}$ ARE MULTIPLIED BY 10^3 .

Mode [i]	g [arcsec/yr]	β [deg]	$e_{A,i}$	$e_{B,i}$	$e_{C,i}$	Period [yr]
1	209.991	272.28	-2.075	21.148	-20.311	6171.7
2	44.713	140.17	-8.146	0.010	0.013	28984.7
3	14.061	333.01	-6.928	-7.937	-7.960	92169.0

TABLE 3
FUNDAMENTAL FREQUENCIES AND PERIODS IN THE PSR 1257+12 SYSTEM.

Frequency (period) [i]	1	2	3
n_i [deg/d]	14.249 (25.264 d)	5.410 (66.544 d)	3.665 (98.218 d)
g_i [arcsec/yr]	197.696 (98502.1 yr)	43.881 (29534.0 yr)	13.157 (6555.5 yr)
s_i [arcsec/yr]	-44.023 (29439.3 yr)	-203.108 (6380.9 yr)	0 (-)

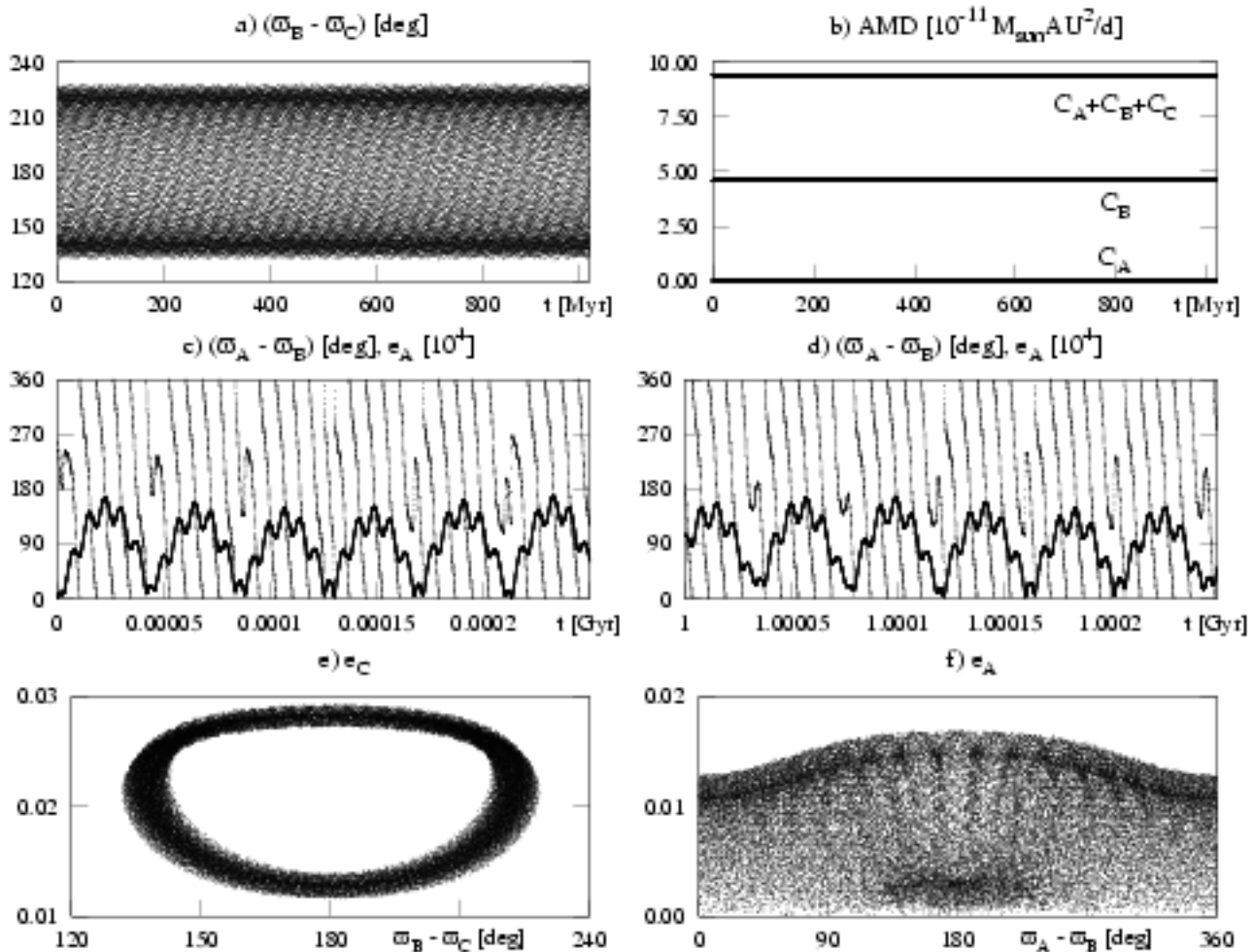


FIG. 2.—

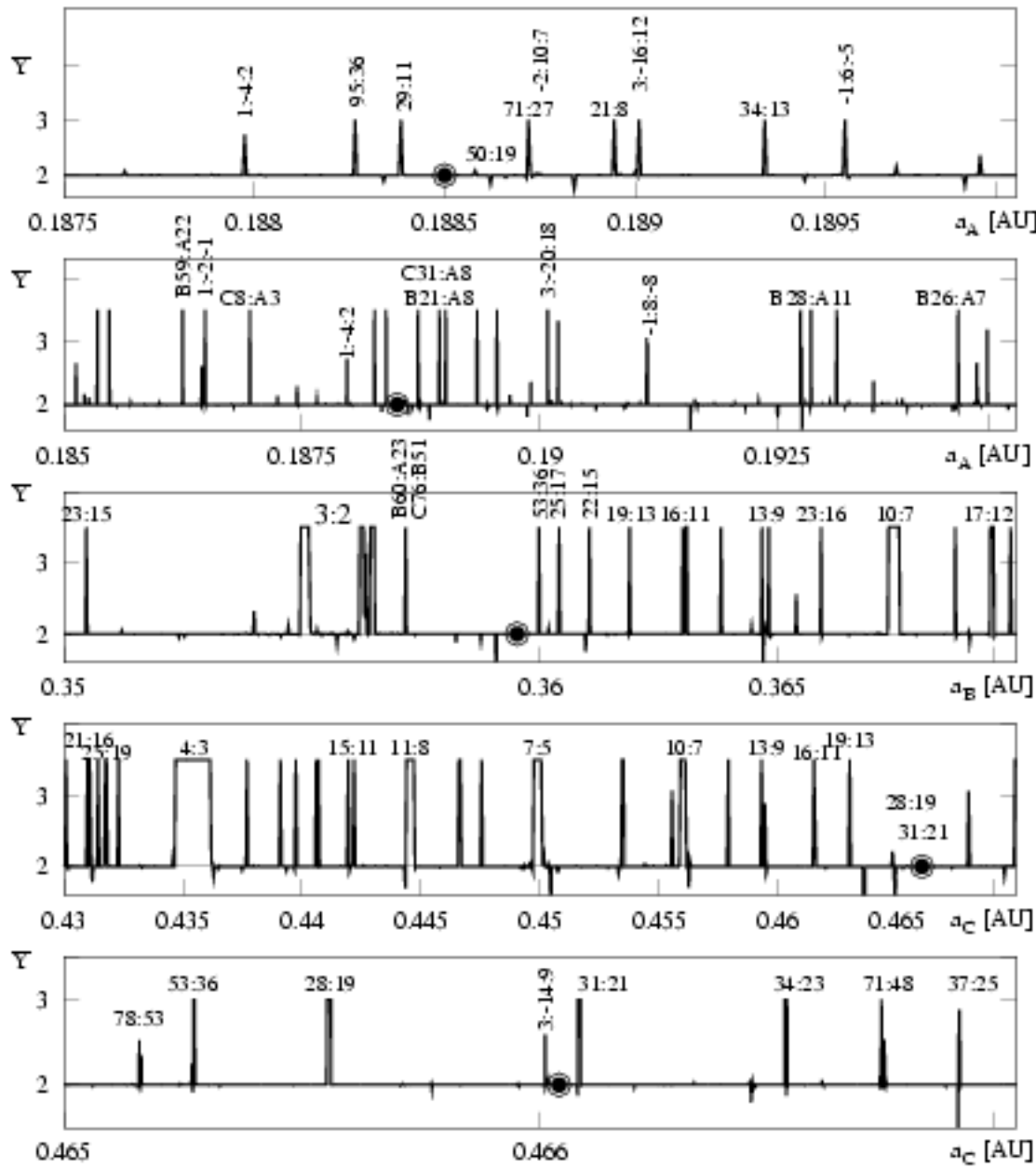


FIG. 3.—

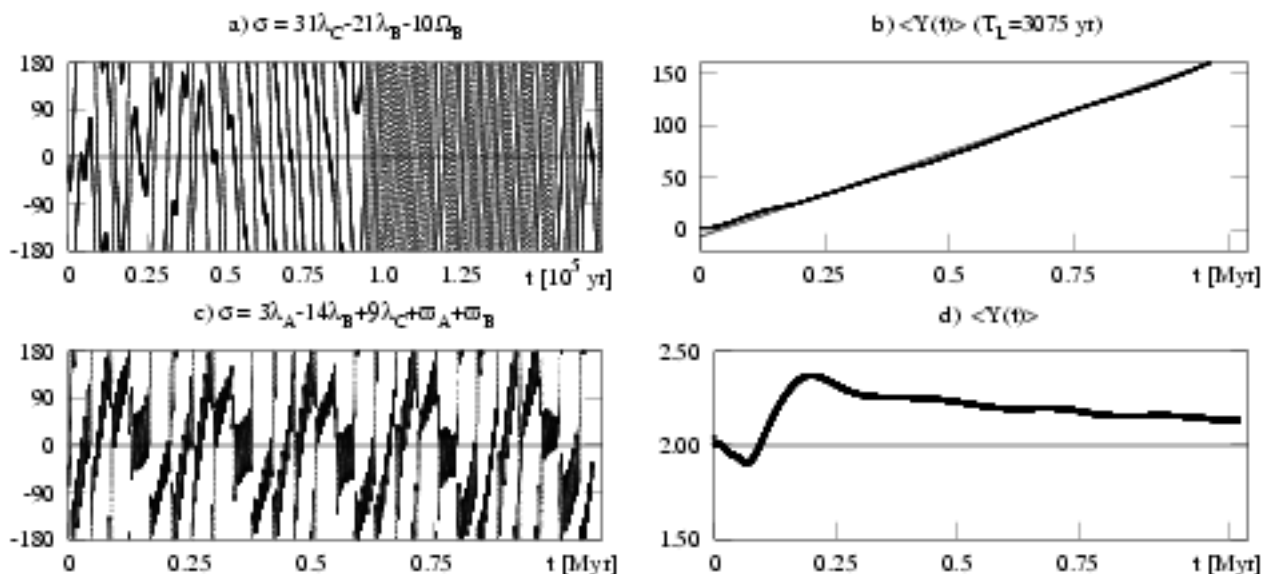


FIG. 4.—

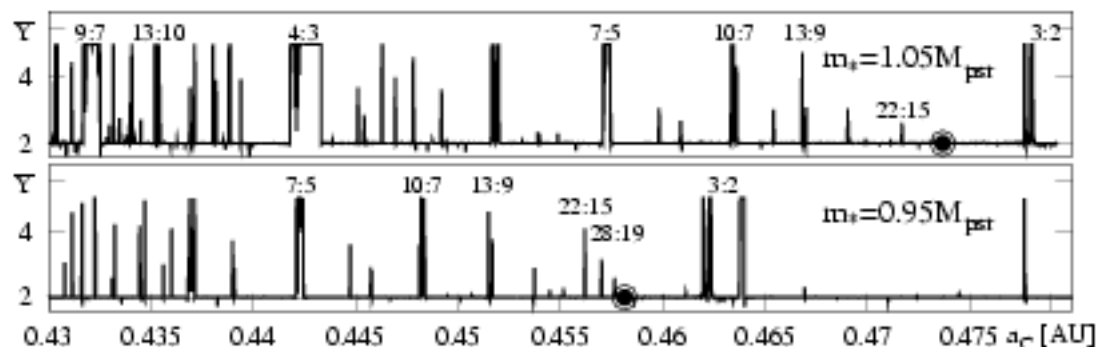


FIG. 5.—

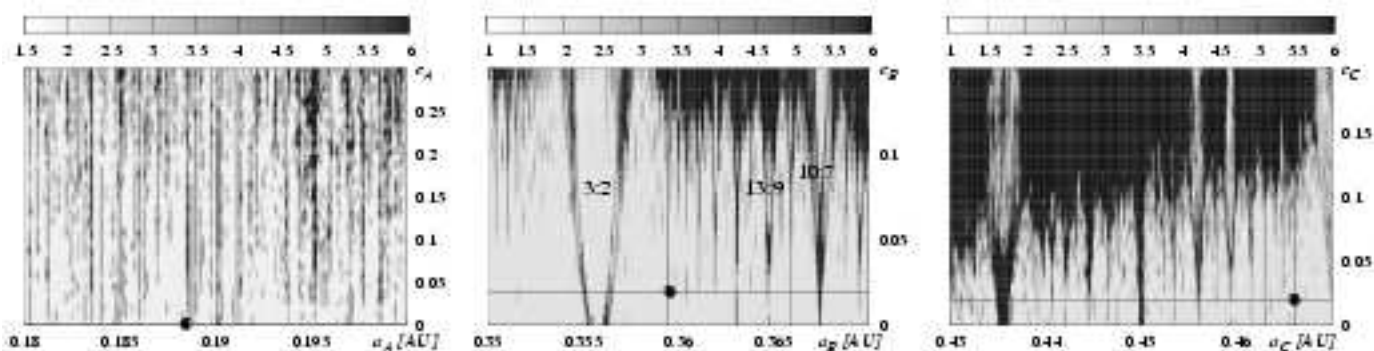


FIG. 6.—

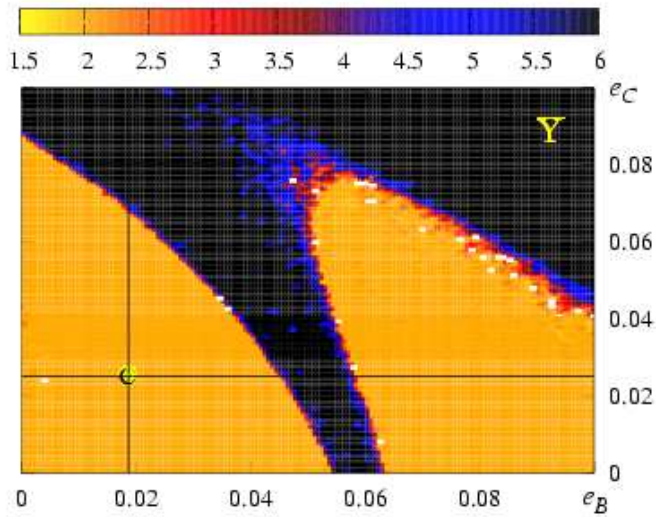


FIG. 7.—

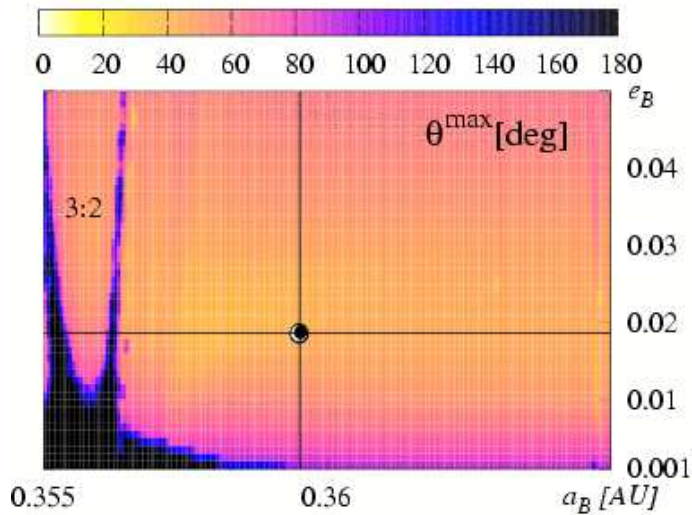


FIG. 8.—

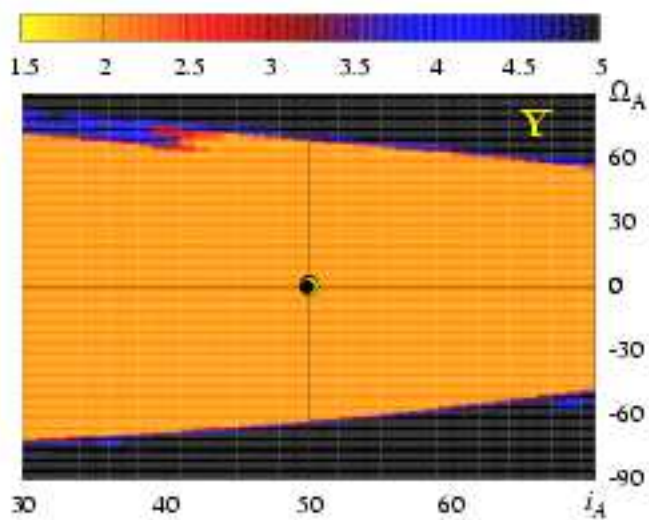


FIG. 9.—

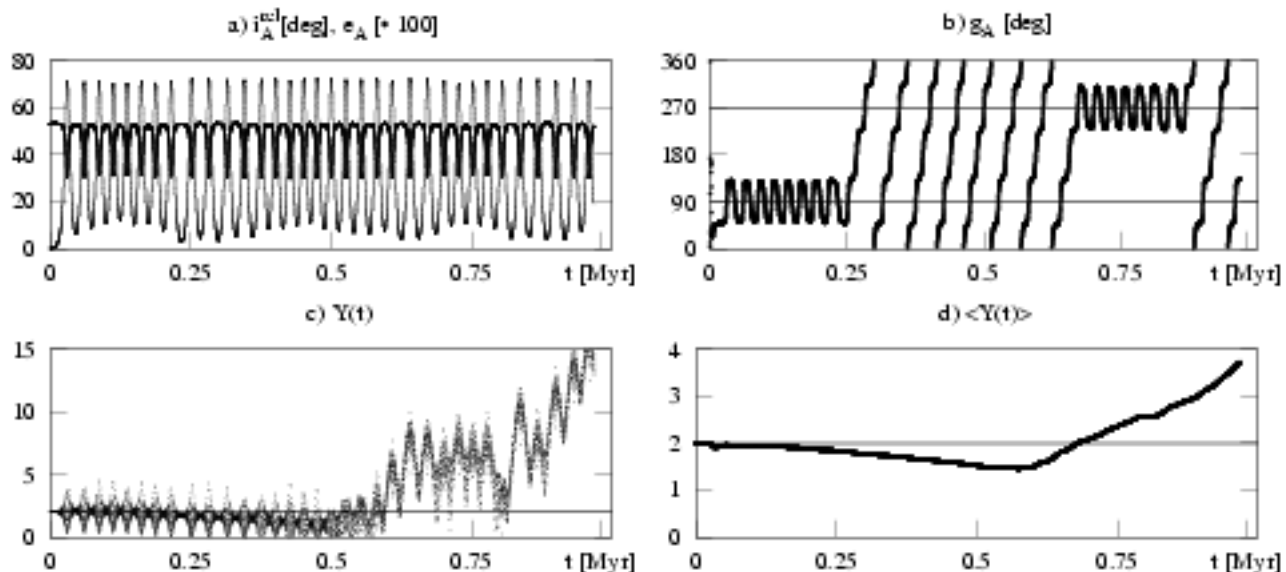


FIG. 10.—

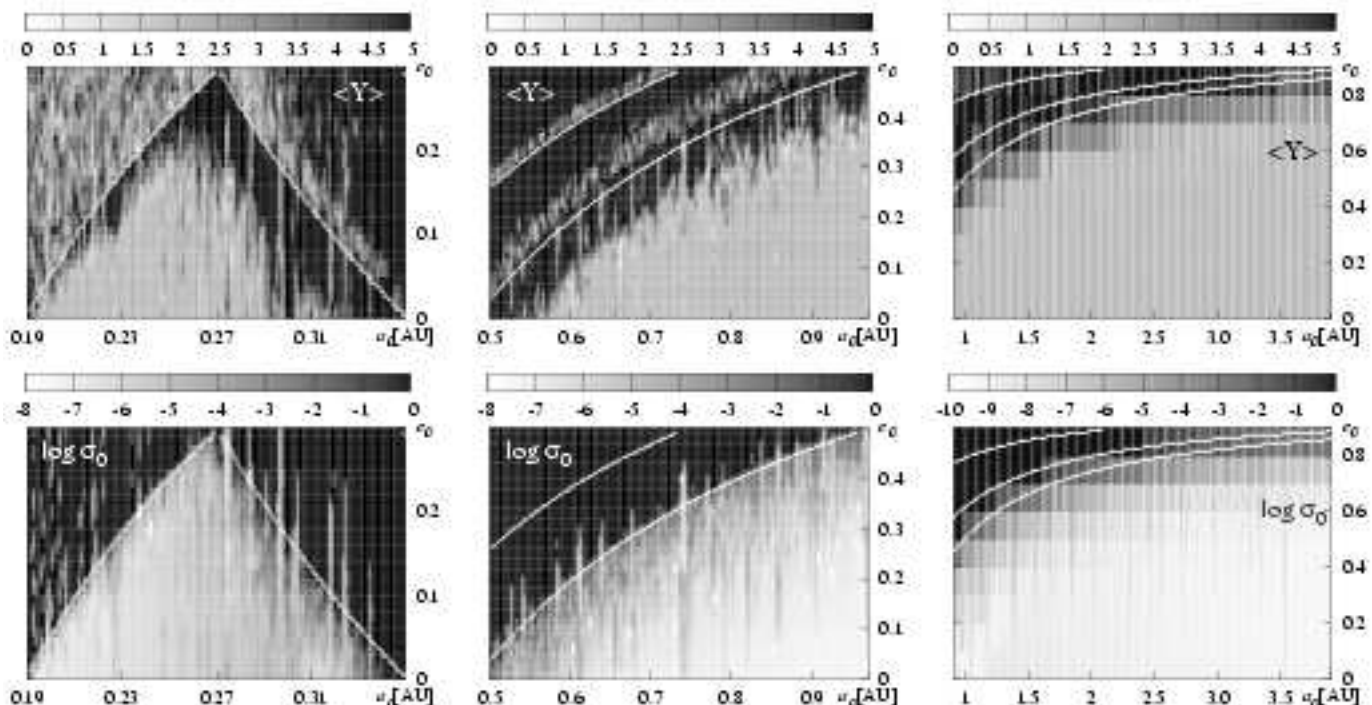


FIG. 11.—

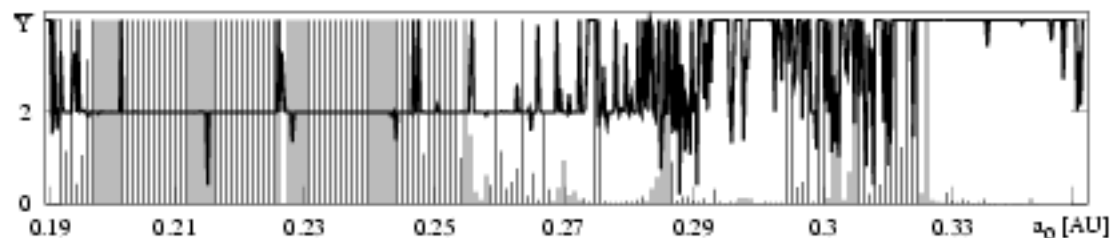


FIG. 12.—

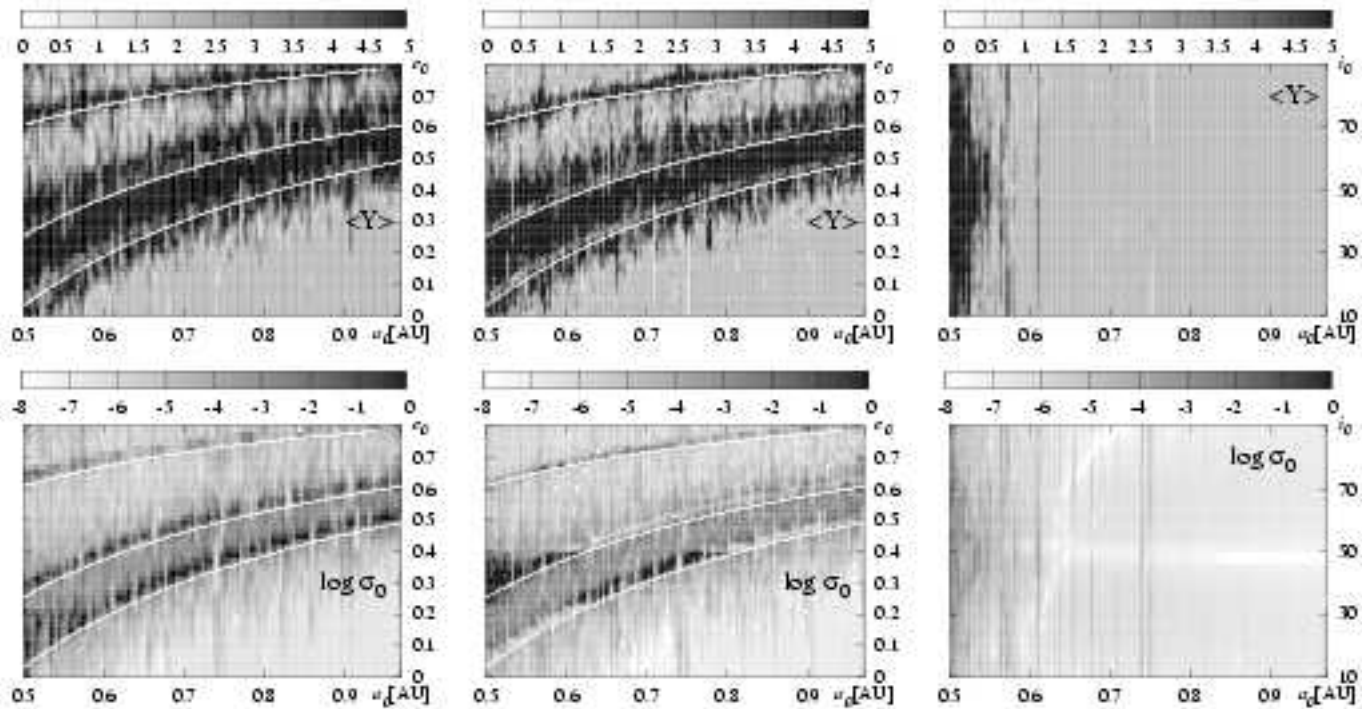


FIG. 13.—